Appl. Phys. A (2017) 123:408
DOI 10.1007/s00339-017-1017-z

Applied Physics A
Materials Science & Processing

Influence of chemical composition on the X-ray photoemission, thermopower, specific heat, and magnetic properties of $CeNi_2(Si_{1-y}Ge_y)_2$

T. Toliński[1] · K. Synoradzki[1] · A. Bajorek[2] · G. Chełkowska[2] · M. Koterlyn[3,4] · G. Koterlyn[5] · R. Yasnitskii[4]

Received: 24 October 2016 / Accepted: 4 May 2017 / Published online: 12 May 2017

Abstract We report our studies of the intermediate compositions between $CeNi_2Si_2$ and $CeNi_2Ge_2$, i.e., the alloys $CeNi_2(Si_{1-y}Ge_y)_2$ by means of the thermopower, electrical resistivity, specific heat, magnetic susceptibility, and X-ray photoemission measurements. $CeNi_2Si_2$ is a fluctuating valence system and $CeNi_2Ge_2$ is known to show the heavy fermion behaviour. The change of the temperature dependence of the resistivity towards the typical metallic behaviour occurs below y 0.25. The transition between $CeNi_2Si_2$ and $CeNi_2Ge_2$ is discussed in the frames of competition between the crystal electric field and Kondo interactions. It is found that valence stabilisation occurs for Ge content $y > 0.25$. The hybridization energy Δ determined from the XPS Ce 3d spectrum reflects well the behaviour of the parameter E_{ex} obtained from the analysis of the magnetic susceptibility by the interconfiguration fluctuation model. It has been also shown that thermopower data can be successfully described employing the single ion model for $0.6 < y < 1.0$ and two-band model including the crystal electric field splitting for $y \leq 0.25$.

✉ T. Toliński
tomtol@ifmpan.poznan.pl

[1] Institute of Molecular Physics, Polish Academy of Sciences, Poznań, Poland

[2] Institute of Physics, Silesian University, Uniwersytecka 4, 40-007 Katowice, Poland

[3] Institute of Physics, K. Wielkiego University, Bydgoszcz, Poland

[4] Faculty of Electronics, Ivan Franko National University of L'viv, L'viv, Ukraine

[5] Western Scientific Center, National Academy of Sciences of Ukraine and Ministry of Education and Science of Ukraine, L'viv, Ukraine

1 Introduction

The compounds of the composition MT_2X_2 (M—Ce, U; T—transition metal; X—Si, Ge) are known to exhibit many of the anomalous behaviours resulting from the hybridization between the f electrons and the conduction states. It includes heavy fermions (HF), superconductivity, fluctuating valence, magnetic ordering, and non-Fermi-liquid (NFL) behaviour [1–5].

We have investigated physical properties of compositions intermediate between $CeNi_2Si_2$ and $CeNi_2Ge_2$, i.e., the alloys $CeNi_2(Si_{1-y}Ge_y)_2$. While $CeNi_2Si_2$ is a well confirmed fluctuating valence (FV) system [2, 6, 7], the behaviour of the HF $CeNi_2Ge_2$ indicates on exotic behaviours like NFL and superconductivity [8–15]. It is due to the proximity of this compound to the antiferromagnetic Quantum Critical Point (QCP). The Kondo temperature of $CeNi_2Ge_2$ is about 30 K and the onset of superconductivity is strongly sample-dependent and still not confirmed as a bulk effect [10].

In the present study it is shown that the combination of effects like the valence change, Kondo temperature reduction and the neighbourhood of the crystal electric field excitations leads to a strong dependence of the physical properties on the Ge content.

2 Experimental

The polycrystalline samples of $CeNi_2(Si_{1-y}Ge_y)_2$ have been prepared by arc-melting of the constituent elements in a purified argon atmosphere. Weight losses after melting were below 0.5 mass%. After synthesis the compounds were annealed at 900 K during 120 h. The crystal structure was verified by X-ray diffraction technique using the Co

Kα radiation. The full-pattern Rietveld refinement confirmed the tetragonal body-centered $ThCr_2Si_2$-type structure, space group I4/mm (no. 139) for all the studied compositions.

The thermoelectric power (TEP) was measured using the thermal transport option (TTO) of the PPMS commercial device (Quantum Design). To use the four-probe method, bar-shaped samples were obtained with a wire saw. For these same samples the dc electrical resistivity was measured.

Heat capacity measurements were carried out on the PPMS in the temperature range 1.9–400 K, by the relaxation method using the two-τ model.

The magnetic dc susceptibility has been measured using the VSM option of the PPMS device including the oven option for measurements up to 1000 K.

The XPS measurements were performed with the use of PHI 5700/660 Physical Electronics spectrometer. The spectra were analysed at room temperature using monochromatized Al Kα radiation (1486.6 eV). The samples were fractured and measured in vacuum of 10^{-10} Torr.

The stoichiometry of the samples was verified by Energy Dispersive X-ray Spectroscopy (EDS). Figure 1 provides exemplary pictures of the tested samples showing that the nominal stoichiometry is close to the stoichiometry derived from EDS averaged over selected areas of the samples.

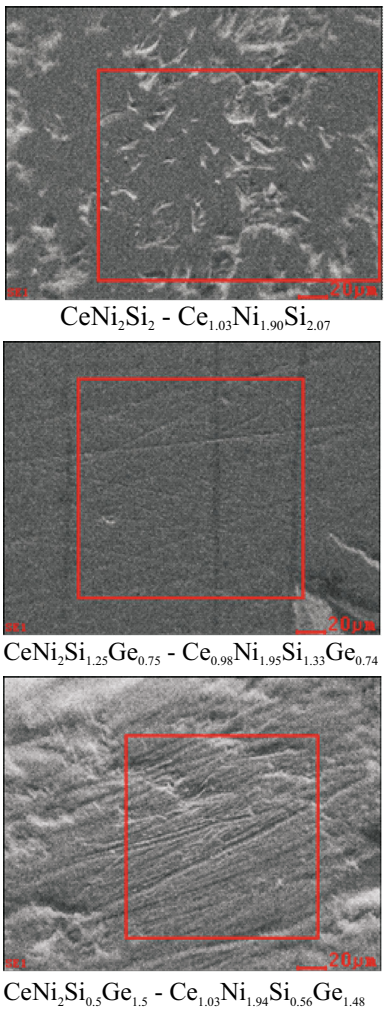

Fig. 1 Examples of the EDS pictures for $CeNi_2(Si_{1-y}Ge_y)_2$. Both the nominal stoichiometry as well as the stoichiometry resulting from averaging over the indicated areas (*red squares*) are provided below the pictures

3 Results and discussion

3.1 Structural studies

The X-ray diffraction patterns (Fig. 2) refined with the FullProf Suite packet have confirmed that all the samples are single phase. Moreover, the lattice parameters and the unit cell volume (Fig. 3) follow a linear dependence according to the Vegard's law for all the $CeNi_2(Si_{1-y}Ge_y)_2$ alloys with $y > 0.25$. It implies that the Ce valence is stable for all the compositions with the Ge content above 0.25. The significant deviation of the lattice constants for the parent $CeNi_2Si_2$ compound may be ascribed to its well confirmed fluctuating valence state [2, 6, 7]. Similar valence evolution has been observed for other isostructural series of alloys, e.g., $Ce(Ni_{1-x}Cu_x)_2Si_2$ [16, 17]. Hence, it is interesting to survey the magnetic, transport, and thermodynamic properties of the $CeNi_2(Si_{1-y}Ge_y)_2$ alloys.

3.2 Transport and thermal properties

The normalised resistance data of $CeNi_2(Si_{1-y}Ge_y)_2$ (Fig. 4) reveals that the change of the temperature dependence of the resistivity towards the typical metallic behaviour occurs already below y 0.25, i.e., a tendency to saturation persists up to significant substitutions of Ge by Si. To estimate the magnetic part of the resistivity the Si-based ($y = 0$) compound has been assumed to be dominated by the nonmagnetic contributions. The choice of adequate reference compound is of key importance. We have found that the resistivity curves (not shown) for $LaNi_2Si_2$, $LaNi_2Ge_2$, and $CeNi_2Si_2$ are all rather close each other and the choice of one of them does not influence significantly the position of the resulting peak of the magnetic contribution, which is the main derived parameter. However, we claim that the use of $CeNi_2Si_2$ better reflects the behaviour of the $\Delta\rho(T) = \rho[CeNi_2(Si_{1-y}Ge_y)_2] - \rho[CeNi_2Si_2]$, especially for $y = 0.88$– it is $-\ln T$ above the peak and close to linear dependence below it (inset of Fig. 4), the last being characteristic of NFL, which is also well confirmed in the literature for pure $CeNi_2Ge_2$ [8]. We explain the advantage

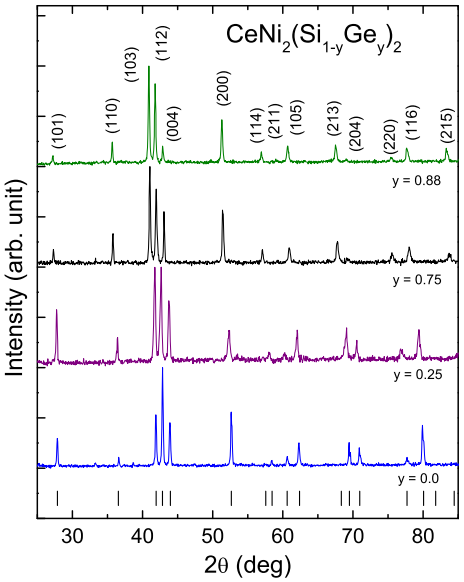

Fig. 2 Representative XRD patterns of the $CeNi_2(Si_{1-y}Ge_y)_2$ ($y = 0.0, 0.25, 0.75, 0.88$) series. The *vertical bars* correspond to the position of the Bragg reflections for $CeNi_2Si_2$

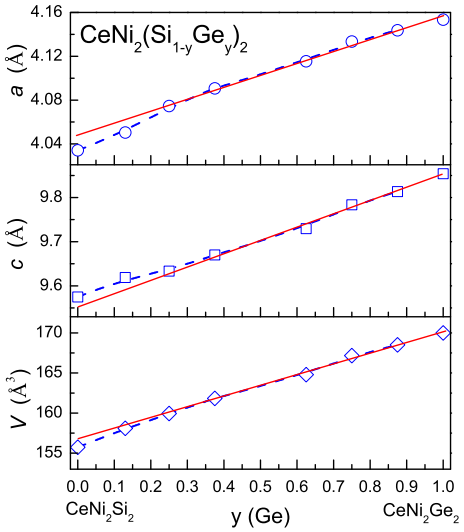

Fig. 3 Lattice parameters and the unit cell volume as a function of the Ge substitution in $CeNi_2(Si_{1-y}Ge_y)_2$. The Vegard's law (*solid line*) is obeyed for all the samples with y > 0.25

of the $CeNi_2Si_2$ reference by the observation that the La-Ni based analogues often show additional non-lattice contributions, e.g., a curvature due to the Mott s–d scattering. We suppose that it is reduced in the Ce-based compounds due to the Ce 4f–Ni 3d electronic transfer, which is responsible for the known fact that Ni is nonmagnetic in many Ce–Ni based compounds, which is also corroborated by the XPS studies discussed at the end of this paper. For La there are no 4f electrons, therefore, Ni may be more effective in the s–d scattering and lead to the additional non-lattice contributions. Moreover, $CeNi_2Si_2$ is a strongly fluctuating

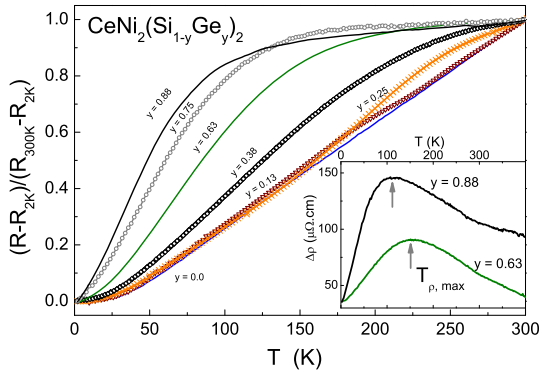

Fig. 4 Normalized electrical resistance measured for various Ge content y. Inset: Examples of the extracted magnetic contribution to the resistivity. It is visible, especially for $y = 0.88$, that the dependence $\Delta\rho$ vs. T is of the type $-\ln T$ above the peak and close to linear below it

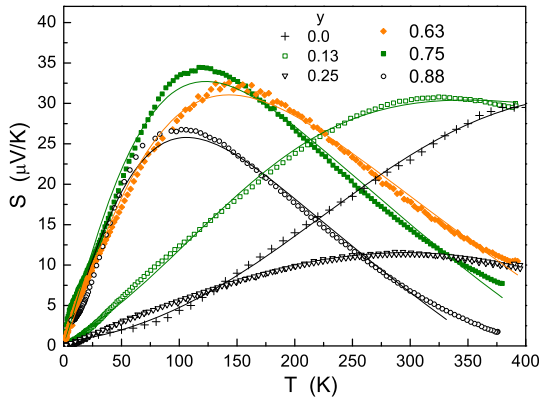

Fig. 5 Temperature dependence of thermopower S for the series of alloys $CeNi_2(Si_{1-y}Ge_y)_2$. The *solid lines* correspond to a fit with Eq. (1) in the range $0.6 < y < 1.0$ and Eq. (2) for $y \leq 0.25$

valence system, hence it is, fortunately, close to a normal metal, at least at temperatures below 400 K, where we perform the analysis.

The above subtraction procedure provides a maximum in resistivity, which changes with y in a manner plotted in Fig. 7. It is consistent with the behaviour of the thermoelectric power. Small differences appear because for a few samples (Ge contents) a well resolved peak in resistivity and/or thermopower could not be observed. The position of the maximum in $S(T)$ presented in Fig. 7 for the $CeNi_2(Si_{1-y}Ge_y)_2$ alloys was extracted from the temperature dependences of thermopower plotted in Fig. 5. In the case of $y = 0$ and $y = 1$ the positions are adapted from literature [6, 7, 14].

The $S(T)$ dependences for $0.6 < y < 1.0$ have been analysed within the frames of the two-band model, i.e., a scattering of conduction-band electrons by a 4f quasiparticle band. The solid lines in Fig. 5 correspond, for $0.6 < y < 1.0$, to a fit with the equation:

$$S(T) = \frac{2}{3}\frac{k_B}{|e|}\frac{\pi^2 E_f T}{(\pi^2/3)T^2 + E_f^2 + W_f^2} + aT, \quad (1)$$

where E_f and W_f are the position and width of the *f*-band in Kelvins. Equation (1) can be rewritten [2] in the course of T_K using the relations: $E_f = T_K$, $W_f = \pi T_K/N_f$, where N_f is the orbital degeneracy $2J + 1$. We have recently assumed [18] that for the energy scale dominated by the crystal electric field the linewidth in Eq. (1) is determined mainly by T_{CEF}, i.e., $W_f = \pi T_{CEF}/N_f$. The second term in Eq. (1) corresponds to other than the Kondo and CEF contributions, e.g., the Mott's diffusion term.

For $y \leq 0.25$, as stems from the deviation of the lattice parameters shown in Fig. 3, the fluctuating valence regime begins and the CEF effects are reduced, therefore, the solid lines in Fig. 5 for $y \leq 0.25$ correspond to a fit with the single-ion Kondo model [19]

$$S(T) = \frac{\pi^2 M(M+1)\sin(2\delta_v)}{\left(\ln^2(T_K/T) + \pi^2 M(M+1)\right)^{3/2}} + aT, \quad (2)$$

where M is the effective spin moment and δ_v is the potential scattering phase shift. The parameters T_K and T_{CEF} are plotted in Fig. 7, values of a, M, and δ_v are of the order of -5×10^{-8} μV/K^2, 0.14, and 0.002, respectively.

It is visible, especially in the case of resistivity, that above $y = 0.25$ the value of T_{max} is strongly reduced. It seems to be an overlap of several effects activated above this Ge content. First, the linear dependence of the lattice parameters is well established for $y > 0.25$, which may stem from the damping of the valence fluctuations (FV) and, therefore, well established localization of the 4f states. It can imply an increase of the effective mass, which is really found and will be discussed below. Second, a crossing of the energy scales connected with the crystal electric field levels and the Kondo interactions occurs around $y = 0.25$. Hence, the complementary specific heat measurements have been carried out and are presented in Fig. 6 as C_p/T vs. T. A tiny anomaly at 6.2 K (dotted vertical line) is due to a very small amount of the Ce oxide often appearing in Ce-based alloys. It seems that the sample without dilution ($y = 0$) is more resistant for the oxidation. One could also consider a small amount of $Ce_5Ni_2Si_3$, which has $T_N = 5.7$ K. In Fig. 6 the electronic specific heat coefficient extracted at $T = 2$ K, γ_{2K}, is plotted as a function of the Ge content. The expected increase of γ with the increase of y is clearly visible and has also been observed previously [3, 4, 20]. However, we indicate additionally in Fig. 7 the Kondo temperature estimated from the relation $T_K = 0.68R/\gamma$. As it cannot work well for the FV alloys this recalculation is limited to $y > 0.6$. For FV system a large value of T_K is expected. In various

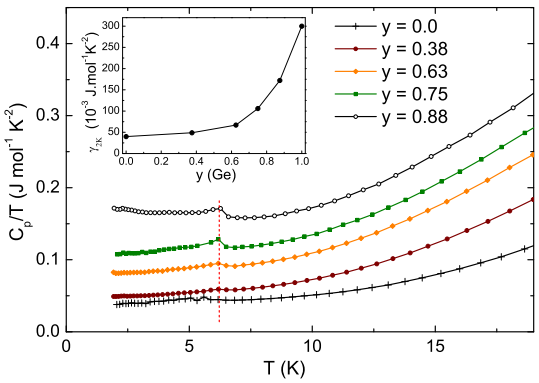

Fig. 6 Temperature dependence of the specific heat C_p/T for the $CeNi_2(Si_{1-y}Ge_y)_2$ alloys. A tiny anomaly at 6 K (*dotted vertical line*) is due to a very small amount of the Ce oxide. Inset: The electronic specific heat coefficient γ_{2K} extracted at $T = 2$ K as a function of the Ge content

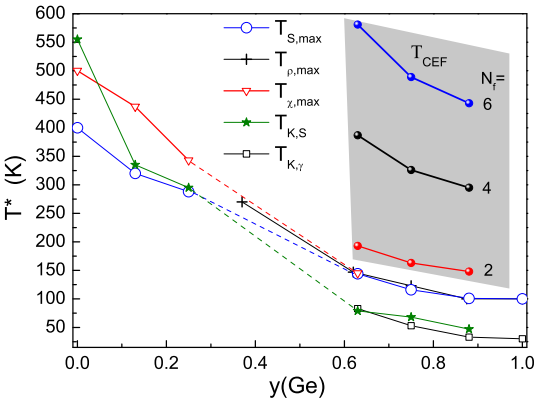

Fig. 7 The temperature of the peak appearing in the resistance ($T_{\rho,max}$), thermopower ($T_{S,max}$), and magnetic susceptibility ($T_{\chi,max}$) as a function of the Ge content. *Dashed lines* are used in the wide *y* range, where the peaks are not visible. Open squares denote the Kondo temperature ($T_{K,\gamma}$) estimated from the relation $T_K = 0.68R/\gamma$ in the range of heavy effective masses $0.6 < y < 1.0$. Stars present the Kondo temperature determined from the thermopower using Eq. (1) in the range $0.6 < y < 1.0$ and Eq. (2) for $y \leq 0.25$. The spheres (*shaded area*) illustrate the CEF split calculated from Eq. (1) assuming three possible degeneracies N_f

estimates provided in literature it varies in the range 400–1200 K for the parent $CeNi_2Si_2$ compound [2, 6, 7].

The spread of the lower crystal electric field level excitations determined in literature for $CeNi_2Ge_2$ by different methods (specific heat [14], inelastic neutron diffraction [21]) ranges between 200 and 300 K. It is in agreement with the estimation of T_{CEF} obtained from Eq. (1) and plotted in Fig. 7 for the case of three possible degeneracies N_f, the closest solution being for $N_f = 2$. One can notice that the crossing of the Kondo and CEF energy scales occurs at y of about 0.25–0.6 explaining the drop or lack of the characteristic temperatures in this y range (Fig. 7). It concerns also the magnetic susceptibility results discussed in next section.

3.3 Magnetic properties

The change from the fluctuating valence in $CeNi_2Si_2$ to the heavy fermion state in $CeNi_2Ge_2$ should noticeably affect the temperature behaviour of the magnetic susceptibility. Figure 8 shows examples of the $\chi(T)$ dependence for $y = 0.13$ and 0.63, which correspond to the FV and HF case, respectively. A broad maximum is visible at 400 K for $y = 0.13$ and in FV systems it is often interpreted using the interconfiguration fluctuation (ICF) model [22–24], which describes the magnetic susceptibility employing the average of the configurations 4f ^{n} and 4f $^{n-1}$, separated by the energy E_{ex}. For the case of cerium the magnetic susceptibility is written as:

$$\chi_{ICF}(T) = \frac{N_A \mu_{eff}^2 [1 - v(T)]}{3k_B \sqrt{T^2 + T_{SF}^2}}, \quad (3)$$

where N_A is the Avogadro's number, $\mu_{eff} = 2.54\ \mu_B$ is the effective paramagnetic moment of Ce^{3+} and $v(T)$ is the mean occupation of the ground state:

$$v(T) = \frac{1}{1 + 6\exp\left[-E_{ex} \Big/ \sqrt{T^2 + T_{SF}^2}\right]}, \quad (4)$$

T_{SF} is the spin fluctuation temperature corresponding to the fluctuation between the magnetic and nonmagnetic valence states of Ce and can be expressed via the rate of fluctuations [25] $T_{SF} = \omega_{SF}/k_B$. It should be noticed that two notations of the effective temperature are used in literature, $(T + T_{SF})$ [23] or $(T^2 + T_{SF}^2)^{1/2}$ [24, 26].The latter can be also interpreted as the broadening of the 4f energy levels and in principle can include different contributions to the spin fluctuations (thermal excitations, quantum mechanical fluctuations, the effect of the 4f-conduction electron hybridization). We have tested both options and similar order of parameters values has been obtained, but $(T^2 + T_{SF}^2)^{1/2}$ provides clearly better quality of the fit, hence better describes the system studied.

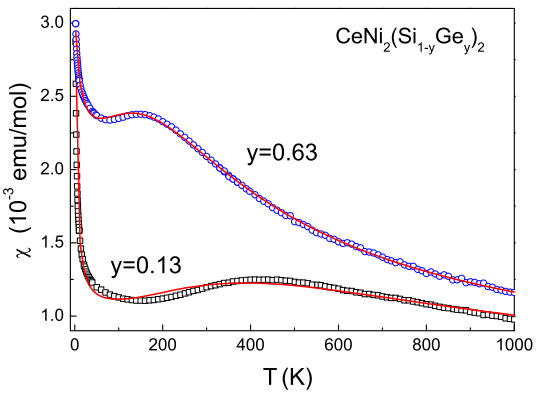

Fig. 8 Temperature dependence of the magnetic susceptibility for $y = 0.13$ and $y = 0.63$. *Solid lines* correspond to the fit with Eq. (5)

Finally, the data in Fig. 8 have been fitted by the equation:

$$\chi(T) = \chi_0 + n\frac{C_{Ce}}{T - \theta} + (1 - n)\chi_{ICF}(T), \quad (5)$$

including a possible fraction n of the impurity Ce^{3+} ions and the temperature independent magnetic susceptibility χ_0. C_{Ce} is the Curie constant of the free Ce^{3+} ion and θ is the paramagnetic Curie temperature. This model is dedicated to FV systems and is applied in Fig. 8 to the $\chi(T)$ data for $y = 0.13$ being close in composition to the archetypal FV $CeNi_2Si_2$ compound. Nevertheless, it appears that the ICF model also works well for $y = 0.63$, which is dominated by heavy fermions properties and the valence fluctuations are expected to be strongly damped. This damping is corroborated by a comparison of the obtained fitting parameters. It stems from Table 1 that the characteristic temperature T_{SF} and the energy E_{ex} are significantly reduced comparing the Si and the Ge-rich compounds, which is expected for the FV-HF transition. Reference to Fig. 7 implies the coincidence of T_{SF} with the maximum observed in the resistivity and thermopower, eliminating the deviation between the magnetic susceptibility results and the other methods. It is clearly seen that T_{SF} is of the order of the Kondo temperature. Moreover, as the transitions between the 4f ^{n} and 4f $^{n-1}$configurations can be induced by the interaction between the conduction and the 4f electrons with a strength $\Delta = \pi N(E)|V|^2$, where $N(E)$ is the density of states and V is the hybridization matrix element, the values of the parameter E_{ex} should be of the order of Δ ($E_{ex} \leq \Delta$) and should show similar changes with the doping y. Such coincidence will be shown below for the X-ray photoemission studies.

3.4 X-ray photoemission

Photoelectron spectroscopy is a powerful technique to investigate the electronic structures of correlated electron systems, providing information about the occupied states. Figure 9 shows exemplary X-ray photoelectron spectroscopy spectra of $CeNi_2(Si_{1-y}Ge_y)_2$ alloys collected in a wide binding energy range up to 1400 eV. A small intensity

Table 1 Parameters values extracted from the fit of magnetic susceptibility to Eq. (5) for two exemplary samples of the series $CeNi_2(Si_{1-y}Ge_y)_2$

y	χ_0 10^{-4} (emu/mol)	θ (K)	n	T_{SF} (K)	E_{ex} (K)
0.13	4.61	−1.7	0.008	310	960
0.63	5.22	−10.8	0.012	154	399

χ_0 temperature independent magnetic susceptibility, θ paramagnetic Curie temperature, n fraction of the Ce^{3+} impurities, T_{SF} spin fluctuation temperature, E_{ex} energy difference between the states 4f^1 and 4f^0

of the O 1s and C 1s peaks suggests high quality of the samples. Figure 10a shows the valence band spectra of the investigated alloys. The main peaks in the valence XPS of $CeNi_2(Si_{1-y}Ge_y)_2$ are located at 1.5 eV and originate mostly from the Ni 3d states with some contribution of Ge 4p and Ce 4f states. Near the Fermi level there is a clearly visible peak that can be assigned to Ce $4f^1$. It does not change significantly with y.

In the Ni 2p spectrum (Fig. 10b), two distinct peaks at binding energies of 853.5(1) eV for Ni $2p_{3/2}$ and 870.7 (1) eV for Ni $2p_{1/2}$ are observed for all samples. These peaks positions are in accordance with those reported for other Ce-Ni compounds [27]; however, the peaks are shifted towards higher binding energy relative to the metallic Ni, suggesting a partial filling of the Ni 3d band due to a strong hybridization between Ni 3d, Ce 4f, Si 2p, and Ge 2p states [28]. In addition, only weak satellites of the Ni 2p peaks can be observed in Fig. 10b, which likely arises from filling of the Ni 3d band and suggests that the magnetic moment on Ni is negligible. The shake up satellites are characteristic of paramagnetic compounds. The presence of the Ni 2p satellite has been attributed to the excitation of a Ni 3d electron into the 4 s unoccupied orbital, occurring simultaneously with the 2p photoemission [29, 30]. Ab-initio calculations on rare earth—Ni compounds usually show that the Ni magnetic moment, if present, is antiparallel to the rare earth magnetic moment [31].

To investigate the Ce valence we have examined the BE range typical of the Ce 4d and 3d states. The BE region from 95 to 130 eV for $CeNi_2(Si_{1-y}Ge_y)_2$ alloys is presented in Fig. 11. For all the samples the Ce 4d band overlaps with the Ni 3 s states, therefore, one cannot see the SO splitting of the Ce 4d states. Moreover, the satellite peaks related to the $4f^0$ band, which suggest an

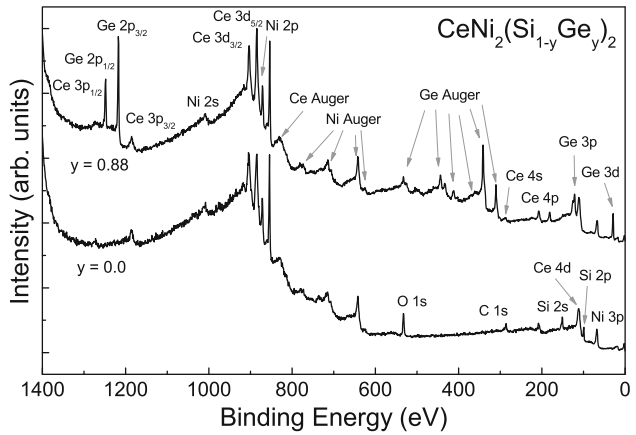

Fig. 9 XPS spectra collected at room temperature within the 0–1400 eV binding energy range (Al Kα radiation) for selected $CeNi_2(Si_{1-y}Ge_y)_2$ alloys

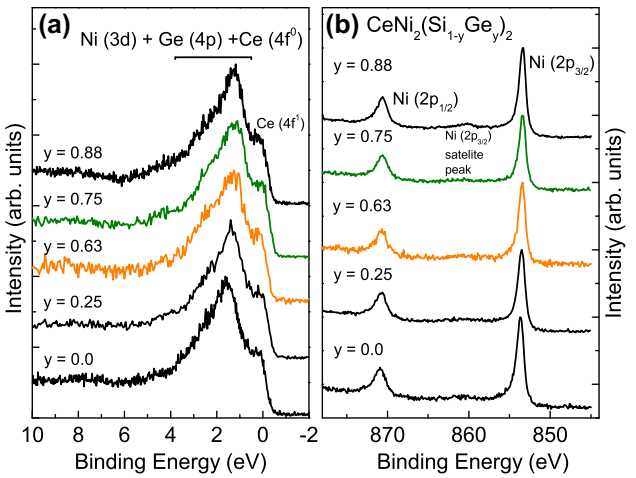

Fig. 10 **a** Valence XPS bands and **b** Ni2p core level spectra for $CeNi_2(Si_{1-y}Ge_y)_2$ alloys

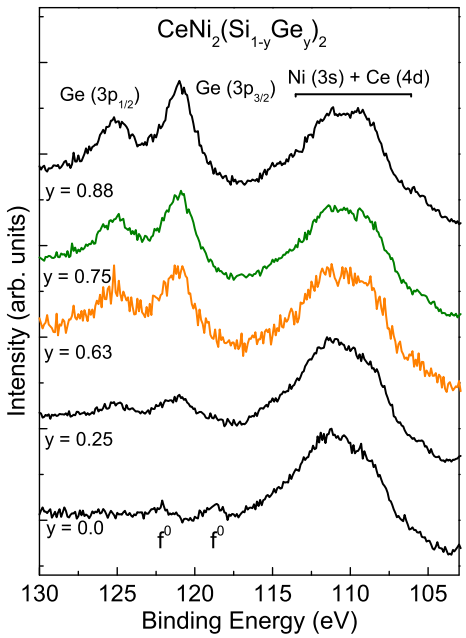

Fig. 11 XPS Ce 4d spectrum of the $CeNi_2(Si_{1-y}Ge_y)_2$ alloys

intermediate valence behaviour of Ce, are clearly visible only for the sample without Ge ($y = 0.0$). In Ge-rich samples those states are absent and/or covered by Ge 3p peaks, with the spin orbit splitting of 4 eV, which is in agreement with a pure Ge.

Figure 12 shows the Ce-3d core level spectra of the $CeNi_2(Si_{1-y}Ge_y)_2$ alloys. For all samples the contributions of the final states $4f^1$ and $4f^2$ are clearly observed, with the SO splitting of 18.8 eV. The f^0 component is present only for the Si-rich samples and indicates the intermediate valence character of the Ce ions. Hence, these observations are consistent with the fluctuating valence state deduced from the Ce 4d spectra.

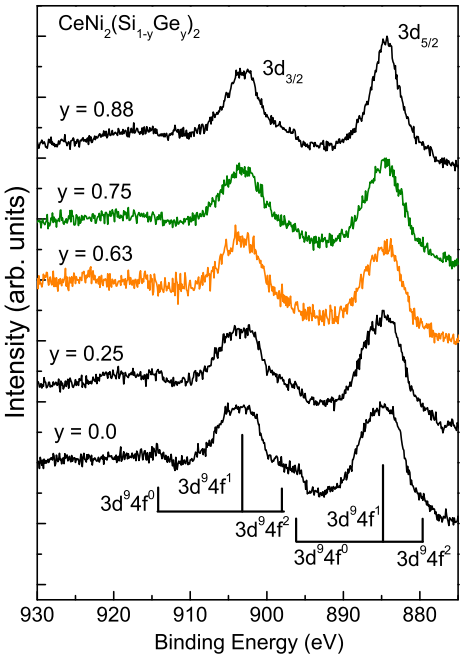

Fig. 12 The 3d XPS spectra of cerium in the $CeNi_2(Si_{1-y}Ge_y)_2$ alloys. f^n ($n = 0,1, 2$) designs the final states related to the main peaks and the satellites. The $3d_{5/2,3/2}$ bands result from the spin–orbit splitting

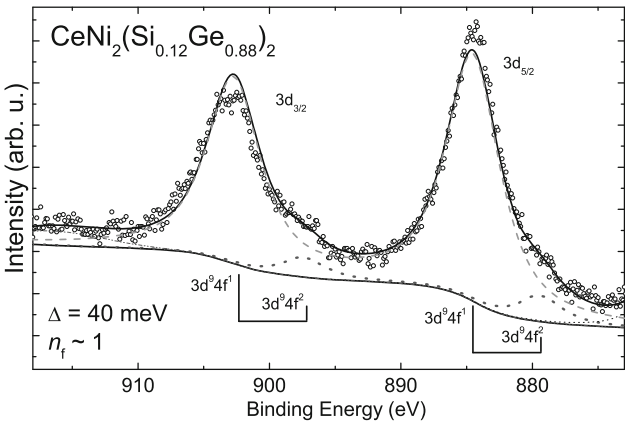

Fig. 13 Deconvolution of the XPS spectrum of the spin–orbit split $3d_{5/2,3/2}$ doublet for the example of the $CeNi_2(Si_{0.12}Ge_{0.88})_2$ alloy. *Open circles* correspond to the experimental spectrum and the *continuous curves* to the fitting results, which is the sum of the $3d^94f^1$ satellites (*dashed line*), $3d^94f^2$ satellites (*dotted line*), and Shirley-type background [34] (*solid base line*). The $3d^94f^0$ satellites are not present, therefore, are not included in the deconvolution

The Ce3d spectra have been analysed on the base of the theoretical model proposed by Gunnarsson and Schönhammer [32, 33] and the exemplary deconvolution is presented in Fig. 13. The f^2 peak intensity reflects well the hybridization strength, therefore, the energy coupling Δ between the f electrons and conduction states can be derived from the intensity ratio $r_2 = I(f^2)/[I(f^1) + I(f^2)]$. The 4f-occupancy n_f can be estimated from the ratio $r_0 = I(f^0)/[I(f^0) + I(f^1) + I(f^2)]$, because the f^0 satellite provides information on the f-electron counts. The value of $n_f = 1$ is attributed to the stable Ce^{3+} state, in the case of the fluctuating valence character of the Ce ions $n_f < 1$. The obtained values are in good agreement with the previous Ce L_3-edge spectra measurements [20]. For $y = 0$ we have obtained $\Delta = 200$ meV and $n_f \approx 0.83$. The latter grows to about 0.9 for $y = 0.25$ and is close to 1 for $y > 0.25$. As the values of Δ are of the order of 2000 K for small y and 400 K for large y (Fig. 13) one can notice that both the order of the values and their behaviour with y reflect the case of the parameter E_{ex} (see Table 1). It clearly shows the agreement between the presented magnetic and photoemission studies.

4 Conclusions

In summary, a very good agreement of the temperature position of the maximum in thermopower and resistivity has been observed and a small deviation in the case of the magnetic susceptibility is eliminated if characteristic temperature T_{SF} is determined based on the ICF model. Surprisingly, the ICF model works well not only for the fluctuating valence, but also for the heavy fermion representatives of the $CeNi_2(Si_{1-y}Ge_y)_2$ series.

The position of the maximum drops is hardly visible for $0.25 < y < 0.63$, especially in the case of the magnetic susceptibility. It has been explained by crossing of the energy scales determined by the Kondo interactions and the crystal electric field excitations. This behaviour coincides also with the change of the valence of the Ce ions, which has been corroborated by the y dependence of the lattice constants and the X-ray photoemission measurements. The hybridization energy Δ determined from the analysis of the XPS Ce 3d spectrum shows the order of values and the changes with y similar to the case of the energy E_{ex} obtained from the ICF model.

It has been shown that the single ion model works well for interpretation of the TEP maximum in the fluctuation valence regime ($y \leq 0.25$), but for large Ge doping a model including the crystal electric field splitting of the ground state yields more reasonable output parameters.

It is found that below the resistivity maximum for $y = 0.88$ a linear temperature dependence of the magnetic resistivity is observed being a sign of the non-Fermi-liquid behaviour, which probably occurs because of the proximity to the quantum critical point. Above the maximum a dependence of the type $-\ln T$ appears.

References

1. T. Endstra, G.J. Nieuwenhuys, J.A. Mydosh, Phys. Rev. B **48**, 9595 (1993)
2. M.D. Koterlyn, R.I. Yasnitskii, G.M. Koterlyn, B.S. Morokhivskii, J. Alloys Compd. **348**, 52 (2003)
3. G. Knebel, M. Brando, J. Hemberger, M. Nicklas, W. Trinkl, A. Loidl, Phys. Rev. B **59**, 12390 (1999)
4. M. Takeuchi, M. Funane, Y. Isikawa, T. Mizushima, T. Tayama, T. Fukuhara, T. Kuwai, J. Phys. Soc. Jpn. **80**, SA063 (2011)
5. F. Failamani, Z. Malik, L. Salamakha, F. Kneidinger, A. Grytsiv, H. Michor, E. Bauer, G. Giester, P. Rogl, Dalton Trans. **45**, 5262 (2016)
6. M.D. Koterlyn, G.M. Koterlyn, R.I. Yasnitskii, Phys. B Condens. Matter **355**, 231 (2005)
7. M. Koterlyn, I. Shcherba, R. Yasnitskii, G. Koterlyn, J. Alloys Compd. **442**, 176 (2007)
8. P. Gegenwart, F. Kromer, M. Lang, G. Sparn, C. Geibel, F. Steglich, Phys. Rev. Lett. **82**, 1293 (1999)
9. R. Küchler, N. Oeschler, P. Gegenwart, T. Cichorek, K. Neumaier, O. Tegus, C. Geibel, J.A. Mydosh, F. Steglich, L. Zhu, Q. Si, Phys. Rev. Lett. **91**, 066405 (2003)
10. C. Bergmann, H.S. Jeevan, M. Schubert, C. Geibel, P. Gegenwart, Phys. Status Solidi B **247**, 694 (2010)
11. D. Ehm, F. Reinert, G. Nicolay, S. Schmidt, S. Hüfner, R. Claessen, V. Eyert, C. Geibel, Phys. Rev. B **64**, 235104 (2001)
12. S. Koerner, E.-W. Scheidt, T. Schreiner, K. Heuser, G.R. Stewart, J. Low Temp. Phys. **119**, 147 (1999)
13. T. Kuwai, M. Takeuchi, T. Tsuchiya, Y. Isikawa, T. Fukuhara, J. Magn. Magn. Mater. **272–276**, 68 (2004)
14. T. Kuwai, P. Sun, T. Sugihara, H. Suzuki, M. Takeuchi, T. Mizushima, A. Mitsuda, Y. Isikawa, T. Fukuhara, Phys. B Condens. Matter **378–380**, 146 (2006)
15. F. Steglich, B. Buschinger, P. Gegenwart, M. Lohmann, R. Helfrich, C. Langhammer, P. Hellmann, L. Donnevert, S. Thomas, A. Link, C. Geibel, M. Lang, G. Sparn, W. Assmus, J. Phys.: Condens. Matter **8**, 9909 (1996)
16. E.V. Sampathkumaran, R. Vijayaraghavan, Phys. Rev. Lett. **56**, 2861 (1986)
17. T. Toliński, K. Synoradzki, M. Koterlyn, G. Koterlyn, R. Yasnitskii, J. Alloys Compd. **580**, 512 (2013)
18. T. Toliński, V. Zlatić, A. Kowalczyk, J. Alloys Compd. **490**, 15 (2010)
19. K. H. Fischer, in *Thermoelectricity in Metallic Conductors*, ed. by F. J. Blatt and P. A. Schroeder (Springer US, Boston, 1978), pp. 295–305
20. G. Liang, M. Croft, Phys. B Condens. Matter **403**, 1482 (2008)
21. B. Fåk, J. Flouquet, G. Lapertot, T. Fukuhara, H. Kadowaki, J. Phys. Condens. Matter **12**, 5423 (2000)
22. L.L. Hirst, Phys. Kondens. Mater. **11**, 255 (1970)
23. B.C. Sales, D.K. Wohlleben, Phys. Rev. Lett. **35**, 1240 (1975)
24. W. Franz, F. Steglich, W. Zell, D. Wohlleben, F. Pobell, Phys. Rev. Lett. **45**, 64 (1980)
25. S. Layek, V.K. Anand, Z. Hossain, J. Magn. Magn. Mater. **321**, 3447 (2009)
26. C. Mazumdar, R. Nagarajan, S.K. Dhar, L.C. Gupta, R. Vijayaraghavan, B.D. Padalia, Phys. Rev. B **46**, 9009 (1992)
27. T. Toliński, A. Kowalczyk, G. Chełkowska, M. Mihalik, M. Timko, Acta Phys. Pol. A **113**, 327 (2008)
28. V. Rednic, M. Coldea, L. Rednic, L.G. Pascut, N. Aldea, S. Pintea, M. Neumann, J. Phys: Conf. Ser. **182**, 012077 (2009)
29. A. Rosencwaig, G.K. Wertheim, H.J. Guggenheim, Phys. Rev. Lett. **27**, 479 (1971)
30. S. Diplas, T. Knutsen, S. Jørgensen, A.E. Gunnæs, T. Våland, T. Norby, A. Olsen, J. Taftø, Surf. Interface Anal. **40**, 826 (2008)
31. T. Toliński, M. Pugaczowa-Michalska, G. Chełkowska, A. Szlaferek, A. Kowalczyk, Phys. Status Solidi B **231**, 446 (2002)
32. J.C. Fuggle, F.U. Hillebrecht, Z. Zołnierek, R. Lässer, C. Freiburg, O. Gunnarsson, K. Schönhammer, Phys. Rev. B **27**, 7330 (1983)
33. O. Gunnarsson, K. Schönhammer, Phys. Rev. B **28**, 4315 (1983)
34. D.A. Shirley, Phys. Rev. B **5**, 4709 (1972)